Numerical Study of Plasma Production in the VASIMR Thruster*†

Oleg Batishchev and Kim Molvig
Massachusetts Institute of Technology
Nuclear Engineering Department
MIT NW16-258
167 Albany St
Cambridge, MA 02139, USA
617-253-5799
batish@mit.edu

IEPC-01-208

Several different models for the numerical analysis of gaseous propellant and collisional plasma inside high Variable Specific Impulse Magnetoplasma Rocket (VASIMR) [1-4] are proposed. Gas and plasma flows are described using time-dependent non-linear kinetic equations, accounting for various collisional processes in the volume and at the material walls in the presence of external magnetic and self-consistent electrical fields and sheaths. An additional zero dimensional power and particle balance model is considered as well. The latter includes 13 ordinary non-linear equations with relevant boundary conditions. This relatively simple model is coupled to a semi-analytical hybrid mixed-collisional pipe flow model taken in the 1D approximation. The numerical results from all the models are benchmarked against current VX-10 data for hydrogen (deuterium) and helium discharges, as given by langmuir plasma probes and retarded probe analyzers (RPA). The numerical data is also used to explain some of the experimental observations. The model is applied to predict helicon plasma source performance in space, including next step VF-10 configuration. Some structural modifications of the thruster are proposed.

Introduction

VASIMR is a unique electrode-free electric propulsion system [1-4], which has a potential of achieving specific impulse on the order of 30Ksec with 50% energy efficiency. Fuel efficiency depends entirely on that of a plasma source. Presently VASIMR project considers helicon discharge plasma source [5,8] a primary candidate.

A typical VASIMR thruster combines three distinct areas i) plasma source, ii) plasma RF-heating cell and iii) magnetic nozzle, as shown in the Fig.1. The most probable propellant is H2 to achieve maximum specific impulse Isp at a given mass fueling rate. There are several important collisional processes taking place in such a thruster. Firstly, there are a few inelastic channels to break incoming molecular gas into neutral atoms, ionization and excitations of neutrals, and wall interactions [6-7].

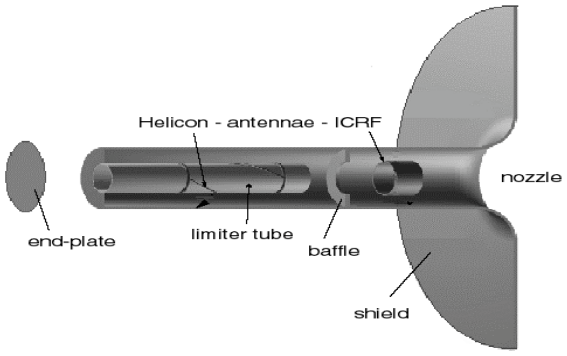

Figure 1 – Gas/plasma facing section of VASIMR thruster

* Presented as Paper IEPC-01-208 at the 27th International Electric Propulsion Conference, Pasadena, CA, 15-19 October, 2001.
†

Next, there are a number of elastic collisions of potential importance: Coulomb interaction, resonance charge-exchange, etc [9-10]. The typical Knudsen number for the different elementary processes varies in a 0.1-10 range, which indicates that the short mean free path limit [6] fails, and a pure kinetic analysis is required [11-12]. There are a few approaches to that.

Comparison of particle-in-cell and finite difference methods shows that the Fokker-Planck approach is computationally more efficient [22]. Particle methods suffer from the intrinsic statistical noise, which occurs because of the limited number of model particles per cell, and it is always 6-8 orders of magnitude larger than the "natural physical" noise. Finite-difference methods are free of the statistical fluctuations in the first place, and allow studying both coarse and fine effects. From the mathematical point of view numerical particle solution is always non-converged (oscillations recede as an inverse square root of the number of trajectories), while grid methods may give a converged solution up to the computer accuracy ~10-14.

Next, finite numbers of particles per cell in the numerical simulation make it impossible to resolve accurately enough an important energetic tail of the electron and ion distribution functions, because the tail is normally exponential function of energy. Practical limit of the resolution (for 10-100K particles per cell) is 3-4 thermal velocities. Time averaging helps for steady-state regimes only. Thus, non-linear time-dependent study of the transient regimes is impossible in principle.

Grid method with a non-uniform mesh in the velocity space allows equally accurate resolution of the cold core and very energetic tail (100 thermal velocities) of the distribution function. These tails are important for plasma diagnostics with probes and neutral beams; they also determine plasma thermal conductivity.

Lastly, in the regimes of interest, regions of sharp spatial gradients of plasma parameters are expected. The universal tool to study such fronts is provided by adaptive grids in space [23]. Particle methods are not compatible with adaptive grids. The reason is quite simple: as dimension of a particular cell is reducing by an order of magnitude, its volume is decreasing by three orders of magnitude. The limited number of model particle per initial volumetric cell becomes proportionally smaller, and as an immediate result the statistical error goes up approaching unsatisfactory level of about 100%. Unlike particle-in-cell methods, Fokker-Planck approach is compatible with the adaptive grids resolution of the velocity space is de-coupled with the spatial resolution.

While the pure kinetic approach is an ultimate goal, in the current work we present results from 0-D plasma chemistry model, which allows us to obtain crucial parameters of the helicon discharge: plasma and neutral species composition, temperatures of all plasma components, energy/particle fluxes out of the plasma source and heat fluxes onto wall. This model is the further development of our original model. New addition includes possibility of lyman-α radiation reflection and recapture, ad well as it artificial reduction to study the energy efficiency of the VASIMR thruster.

This simple 0-D model uses critical information about propellant flow in the system of pipes as given by our 1-D semi-analytical hybrid model, which is also included in the present paper. New fully kinetic 2V2D BGK-type model for a rarified gas flow independently verifies its results in a system of connected channels. Information about plasma flow is taken from our fully kinetic Fokker-Planck model that was described in the previous publications [16-17. Those results are compared to recent RPA data for the ion distribution function obtained for the VX-10 experimental setup.

All the above numerical models are used here to

a) understand operation of the helicon plasma source and ion heating sections of the VX-10 experimental thruster,

b) make predictions for the future space VF-10/25 thruster [4,5], and

c) propose practically feasible suggestions on how to boost fuel and energy efficiencies of the critical elements of the plasma thrusters, based on the VASIMR technology.

Current status of VX-10 [5] experiment shows about 40% fuel efficiency for hydrogen, deuterium and helium discharges when they operate in a high-density mode. It's not clear what determines transition to this important mode. We use a few numerical models to study operational regimes of the helicon plasma source.

Energy and particle balances are studied using 0-dimentional model of gas discharge [16]. The following processes are accounted for hydrogenic discharge: molecule and molecular ion dissociation, neutral ion ionization and excitation, charge-exchange, wall conversion, formation of heavy ions, etc. Model predicts plasma and gas species densities and

temperatures to very close to that measured in the experiment. The model is used to assess effects of gas baffles, vacuum tank, gas pre-heating, altering dimensions of the quartz tube, etc. on the hydrogen and helium discharges performance.

Finally we briefly discuss fully kinetic 1D2V and Fokker-Planck-Boltzmann models of the gas [11,18,24] and plasma flows [12, 25-26]. They account for spatial variation of ambipolar potential and external magnetic field and basic elastic and inelastic collisions. Kinetic simulations show that the distribution functions of both gas and plasma species differ from the Maxwellian due to external heating, non-local transport and trapping in the magnetic field. IDF is in concert with recent RPA measurements [21] Preliminary results indicate that specific impulse on the order of 3-4Ksec is achievable by the helicon source along, and 8-10Ksec with additional ICRF-heating of the ions for the 3-10kW input electrical power.

Kinetic model of collisional gas flow in the gas feed – plasma source sub-system

Previous numerical and theoretical studies [16-17] have indicated that degree of gas ionization in the helicon source is low, on the order of 1%. This fact allows viewing propellant flow in the gas feeding - plasma source system ([19], shown in the Fig.2) as entirely independent of that of plasmas.

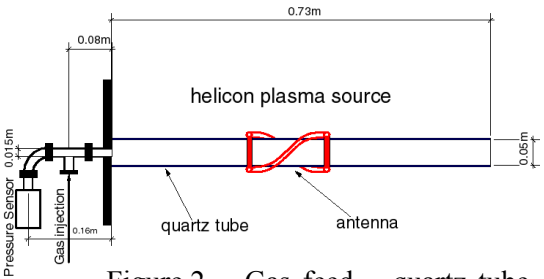

Figure 2 – Gas feed – quartz tube of VX-10 VASIMR configuration

Simple estimate show that gas flow in the system will be strictly laminar. Indeed, from the experimental measurements: pressure drops along the system from PI≈100mtorr in the gas inlet to PVC≈1mtorr in the vacuum chamber, and mass flow rate μ=80sccm we find that the characteristic Reynolds number of the flow

$$Re = V\,d / \nu \approx 20 << Rcr \approx 2300 \qquad (1)$$

is much smaller than the critical value [14], Rcr , which marks the onset of a turbulent regime.

On another hand simple consideration shows that the Knudsen number [13] of the propellant flow

$$Kn = 2\lambda/d \approx 0.5\text{-}2 \qquad (2)$$

Hence, we can view the gas flow to be a composition of the viscous and free molecular laminar flows (as shown in the Fig.3 below).

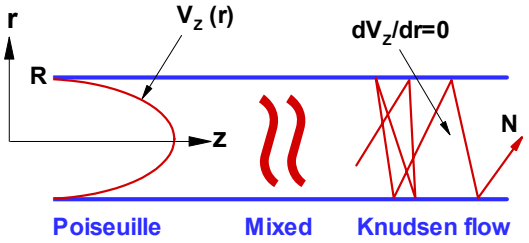

Figure 3 – Scheme of hybrid model

Hybrid Poisseuille - Knudsen model for mixed-collisional gas flow can be easily derived on the basis of two classical results. For the viscous flow one can apply Poisseuille result [14] for a pipe flow: mass throughput in a pipe is proportional to the pressure gradient and to 4-th power of the pipe's radius R:

$$\mu P = A(T)\, R4(z)\, dP/dz \qquad (3),$$

where parameter A(T) contains viscosity, etc.

For a similar free molecular flow one can use analogous result, obtained by Knudsen model [13]:

$$\mu K = B(T)\, R3(z)\, dP/dz \qquad (4),$$

Now, taking into account that mass throughput is constant along axial direction, and that asymptotic expressions (3)-(4) should be valid for the limits Kn→0 and Kn→∞, respectively, we may find the following hybrid expression:

$$\mu = \iota\pi r2\rho\, Vz\, dr = const = \qquad (5)$$

$$\mu P + (\mu K - \mu P)\,[\,1 - \exp\{-Kn\}\,] = C(T,P,z)\, dP/dz$$

where C(T,P,z) is a new composite function. By inverting Eq. (5) we obtain the following finite-difference expression:

$$\Delta P = \mu / c(T,P,z)\, \Delta z \qquad (6),$$

which can be integrated numerically, say from the gas injector (P=PI) up to the end of the quartz tube of the helicon source. Results for He are shown in Fig.4.

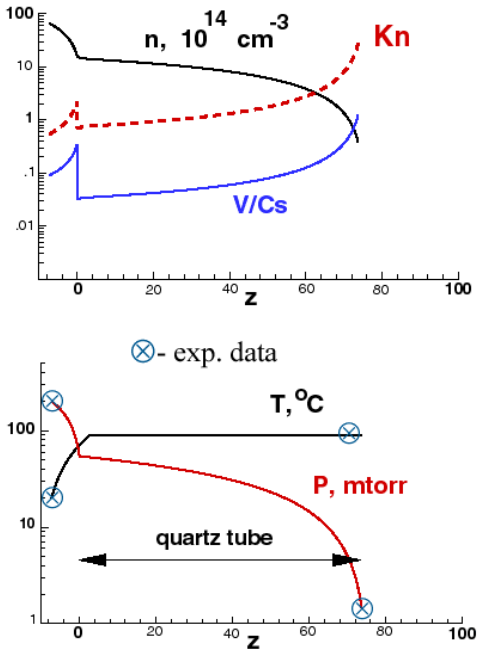

Figure 4 – Profiles of helium gas flow parameters for the VX-10

As one can see from the bottom chart in the Fig.4 agreement with experimental data for the pressure drop along the system are within 1% of accuracy for constant helium flow rate μ=200sccm. Note that axial temperature profile is a fit to the experimental measurements of the quartz tube temperature. We assume that as neutral gas has the same temperature profile due to energy exchange with the wall.

Interestingly enough 80% of the pressure drop occur in the short (8cm) and narrow (1.5cm in diameter), 20% in the quartz tube (Fig.2), and under 1% in the rest sections of the system (magnet bores, etc.). One can see that our original assumption about mixed viscous-free molecular flow is verified a posteriori (as de-facto Knudsen number, Kn, is in the 0.5-5 range).

The helium gas flow experiences transition viscous →molecular → viscous → molecular 3, and accelerates 2 times. What is the most important for our immediate goal is that mean gas flow is very subsonic with average Mach number <M> ≈0.03-0.05.

To crosscheck we benchmark hybrid model against experimental data for molecular hydrogen gas flow at μ=100sccm in the same VX-3 [16] configuration. Corresponding results are close to those in Fig.4.

The major results stay the same: gas flow is very viscous and subsonic, gas density in the center of the quartz tube (where helical antenna is located) is on the order of N≈3-5x1014cm-3.

Comparison of old and new quartz tubes.

Recent results from the VX-10 equipped with a longer quartz tube show two-fold increase of the plasma density in the discharge [19]. We apply 1D model to study gas flow in the original and new tubes. Their geometrical parameters are as follows. Old tube is 5cm in diameter and 70cm long. New tube is 1m long and has slightly larger diameter of 5.5cm.

Though, dimensions of the two tubes are different, surprisingly enough they have the same resistance to the hydrogen gas flow. As one can see from the Fig.5 both pressure and density drops along the tubes coincide with in a few percent. Also in the experiment the RF-antenna position was fixed at the same position closer to the left side of the tube, and the input power stayed the same at about 3 kW.

Thus, the only difference of the two discharges is in the gas density at the location of RF-energy deposition source. With the longer tube the neutral gas density gradient is shallower, energy is released to a more dense gas (and plasma too). Because gas density is higher, we can guess that the ionization may be more efficient, and the discharge will yield more plasma for the equivalent amount of energy transmitted into the electron species.

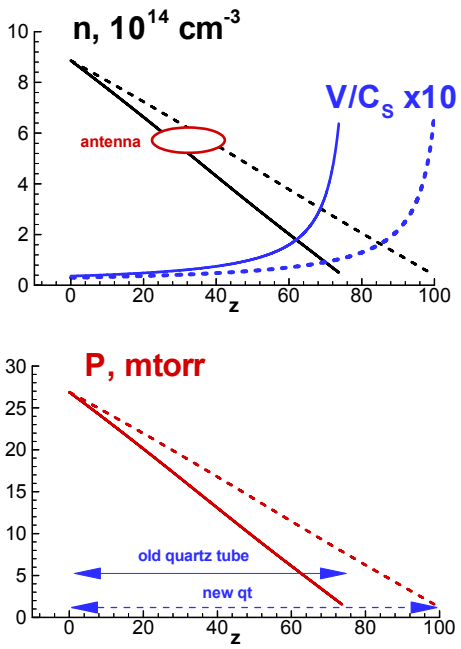

Figure 5 - Gas profiles in old and new tubes

Use of conical tubes instead of cylindrical.

If this theory correct, then we can try to find simple ways to keep neutral gas density higher in the quartz tube volume. One of the possibilities to keep gas density flatter as it accelerates axially – is to use a quartz tube of varying cross-section. Because the helicon RF-antenna has fixed dimensions we propose to use conical shape quartz tubes with average radii approximately equal to that of the internal RF-antenna radius. In this case two-way use of the new tubes becomes possible automatically.

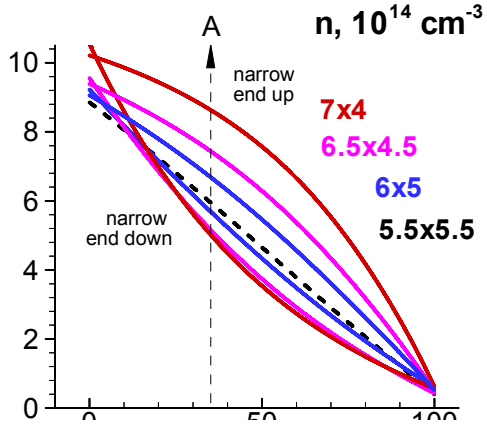

Figure 6 – Gas density in conic tubes

In Fig.6 we present calculated gas density profiles for a set of three tubes with the same length of 1m and the same mean internal radius of 5.5cm. Their small-large radii are as follows: 6x5cm, 6.5x4.5cm and 7x4cm. For comparison we present data for a straight pipe (single linear curve in Fig.6). Each pair of curves – one is folded in and another out – correspond to the same conic-shape tube oriented in two different ways (gas expansion or compression). As one can see simple change of the tube axial orientation allows nearly 100% variation of the gas density in the middle of the pipe. On another hand, when the tube's cross-section is reducing along the flow direction, gas density has much more flat profile. In this case we may expect more efficient gas ionization by electron impact, and higher overall fuel efficiency of the VASIMR thruster. Note that if we'll take into account gas loss due to ionization, the reduction of tube radius has to be large to compensate it. Shaping of the external magnetic field will be obviously required (magnetic choke) to avoid hot magnetized plasma striking the internal surface of the tube, causing energy loses and unwanted damage.

Kinetic model for rarified gas flow

The model considered in the previous paragraph is non-kinetic. Though it gives good agreement with the experimental data, it is semi-empirical. In other words it is based on many experimental data for various non-reacting gas flows at different Knudsen numbers. It's interesting to see if direct kinetic model can give similarly good agreement. Another interesting question is how much actual distribution function will deviate from the usually assumed equilibrated Maxwellian distribution.

Let's consider the system of channels as shown in Fig.7. It resembles the quarts tube and surround it section of the vacuum chamber (Fig.2).

Gas is puffed at the left. At all internal surfaces as shown in Fig.7 gas experiences diffusive reflection (equivalent to a no-slipping boundary condition in gas dynamics). Gas is relatively dense with the Knudsen number for inter-atomic (molecular) collisions in the 0.01-1 range. Typical cross-section for elastic collisions of neutral H(D) species is about 10-15cm2, while gas density varies in the 1013-1016cm-3 range.

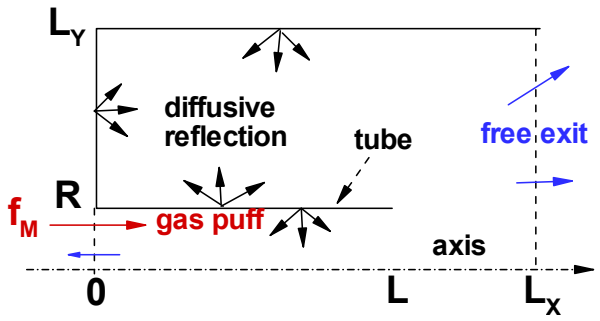

Figure 7 – Model geometry used in a rarified gas flow simulation

In our fully kinetic model all these processes (and 2D spatial transport) are described with a single 4-dimensional kinetic equation for the time-dependent distribution function of gas species.

$$\frac{\partial f}{\partial t}+v_x\frac{\partial f}{\partial x}+v_y\frac{\partial f}{\partial y}=\frac{f_M-f}{\tau(f)}+W+S \qquad (7)$$

More details of the model were presented in our recent works [18, 24]

In the present paper we note only that as a numerical method to solve equation (7) we use splitting, which may be presented in the form of the following 5 steps.

$$\begin{aligned}
&\frac{\partial f}{\partial t}+v_x\frac{\partial f}{\partial x}=0 && (a)\\
&\frac{\partial f}{\partial t}+v_y\frac{\partial f}{\partial y}=0 && (b)\\
&\frac{\partial f}{\partial t}=-\frac{f}{\tau(f)} && (c)\\
&\frac{\partial f}{\partial t}=\frac{f_M}{\tau} && (d)\\
&\frac{\partial f}{\partial t}=\mathrm{W}+\mathrm{S} && (e)
\end{aligned} \qquad (8)$$

Instead of writing down finite difference approximations of each of this terms on the chosen non-uniform meshes, we first find exact analytical for each of the sub-steps in system (8).

For instance, here are the exact solutions for steps (8a) and (8c):

$$\begin{aligned}
&f(t+\Delta,x)=f(t,x-v_x\Delta) && (a)\\
&f(t+\Delta)=f(t)\ \exp\{-\frac{\Delta}{\tau(f(t))}\} && (c)
\end{aligned} \qquad (9)$$

Similar solutions could be easily obtained for the rest sub-steps in the system (8). These analytical solutions are used directly to obtain intermediate solutions. The overall scheme is unconditionally stable and preserves positiveness of the distribution function.
By using special correction procedures for steps (8d) and (8e) the entire method conserves number of particles, momentum components, and the kinetic energy of the gas.

Benchmarking of the kinetic method for gas.

We present results of two tests: back step flow and damping of a shear wave respectively in Figs. 8 and 9. As can be seen from Fig.8. the ratio of the re-attachment length to the step height is about 1.2 – is in agreement with the experimental data [28] for such low Reynolds number flows.

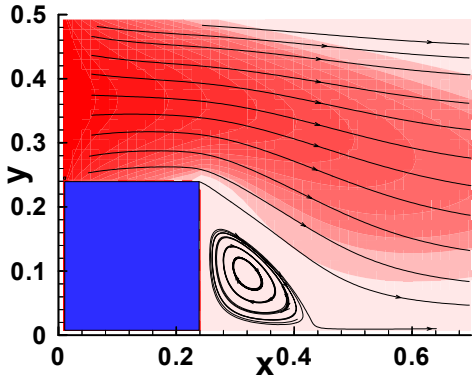

Figure 8 - Back step flow structure

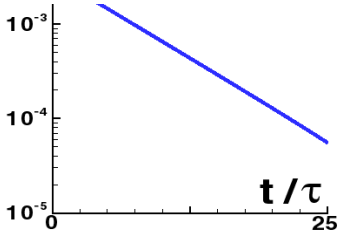

Figure 9 – Exponential decay of the maximum velocity of a periodical shear flow

[15]. The corresponding decrement, γ, for the spatially isothermal and uniform gas with drifting Maxwellian distribution is given by the expression: $\gamma\tau \approx 2\pi^2\lambda^2 / \ ^2$, where λ is mean-free path, and l – wavelength of the disturbance of gas velocity. Numerical result (Fig.9) agrees with theory within few percent for long-wave harmonics. Behavior of the short-wave spectrum is under the investigation.

Results for the rarified gas flow in the VX-10

Gas mass flow scans.

We have varied molecular hydrogen mass flow rate in the 50-200sccm range. The steady-state contours of the gas density are presented in Fig.10 (top) for the lower flow rate. The corresponding contours of the flow velocity are presented is Fig.10 (bottom).

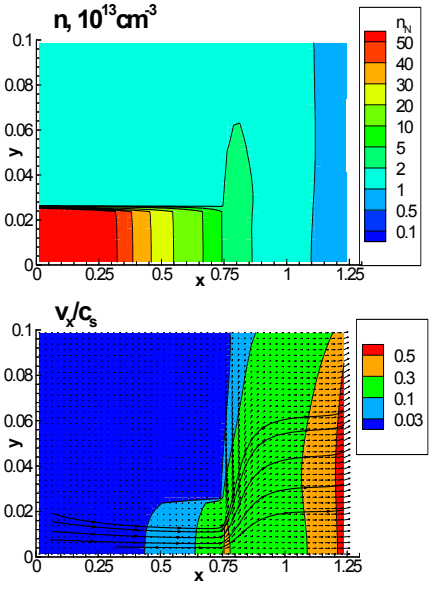

Figure 10 - 50sccm H flow rate

The simi hown in Figs.11. As one can see these results are in agreement with the 1D semi-analytical model, considered above. Indeed, gas accelerates to M~1 at the both boundaries. Also these results verify the need for gas pumping from the outside of the quartz tube. Otherwise, the discharge will occur here due to relatively high residual gas pressure around the helicon antenna, that cam cause its damage.

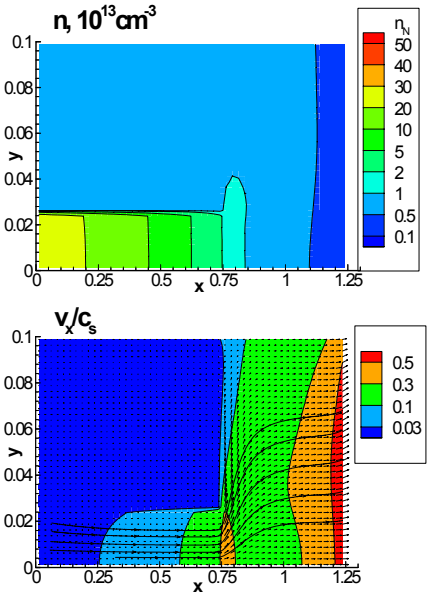

Figure 11 - 200sccm H flow rate

Another interesting observation is concerning the gas distribution function. It is measured at three different locatio e as 11-12) for rate.

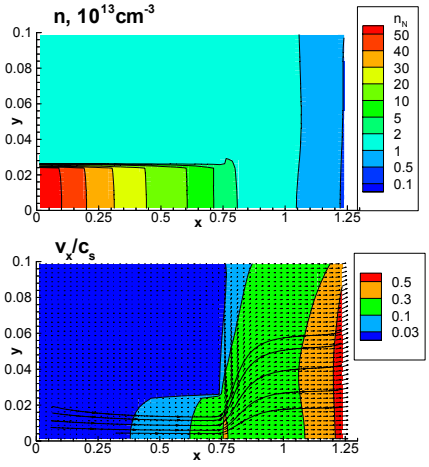

Figure 12 - Results for 100sccm flow rate

In Fig.15 a) and b) we present contours of the gas distribution function right at the symmetry plane inside (1/2 length) the quartz tube (a) and just outside it inside, but starts to deviate from the equilibrium outside the pipe. It is even more non-Maxwellian at half-height of the system, as shown in the Fig.15c. Such strong deviation of the core of the gas distribution function

can affect Doppler measurements of the neutral temperature, and may have other implications.

Addition of gas baffle

Baffling of the gaseous propellant in the plasma source is viewed to be effective for elevating fuel efficiency of the VASIMR thruster. Indeed, our 2D2V kinetic modeling shows that gas density significantly drops for the same upstream conditions.

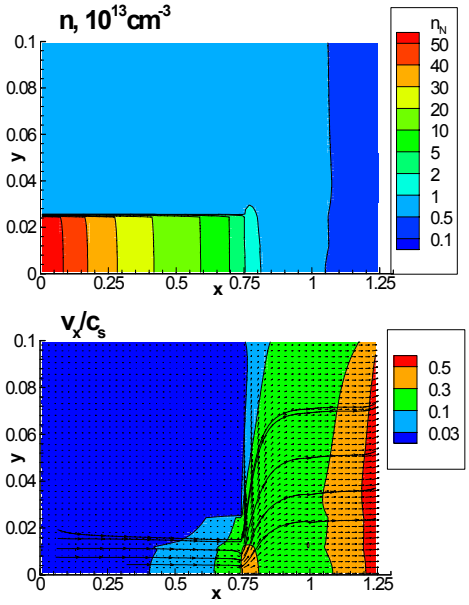

Fig.13. Baffle, 100sccm rate.

The numerical result for a baffle, blocking 70% of the gas flow are shown in Fig.13. They have to be compared to the previous case of gas density and velocity. As one can see, gas density outside the tube dropped twice. Note that the radial baffle is located at the very end of the quartz tube. (We think that conical-shaped tube works as an extended baffle, but may bring other benefits).

The structure of the gas mass flow (*vn*) in the vicinity of the baffle is shown in the Fig. 14. The flow appears to be laminar, with no eddy formed. It accelerates to a sound speed at a small spot, which is localized in the middle of the orifice (Fig.14 (bottom)).

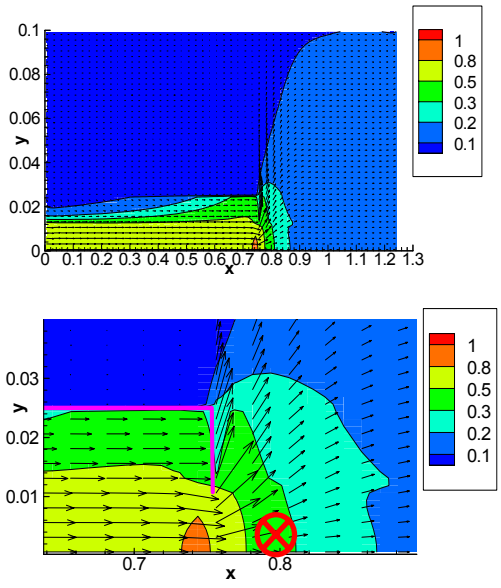

Fig.14. Gas flow structure near the baffle

As ng de on function from the equilibrium. The distribution shown in Fig.15d is teken at the position marked by a cross-mark in Fig.14.

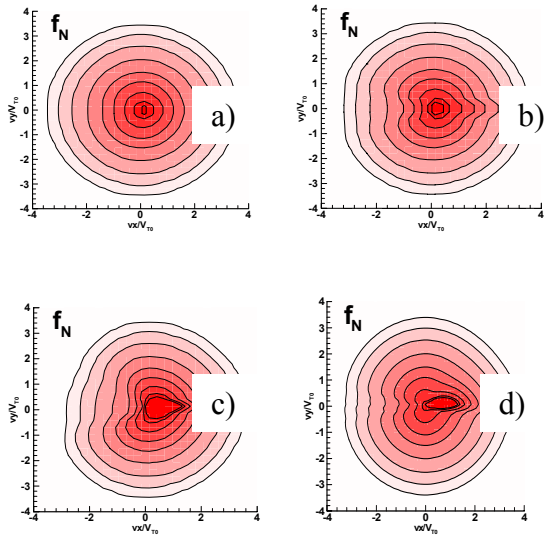

Figure 15 – Gas distribution function at 3 locations in Fig.12: a) – inside q.tube, b) – at the open end of q.tube, c) – (LX,LY/2), and d) – at the marked position in Fig. 14

The helicon has proven to be a robust and efficient plasma source [8]. The helicon source consists of a dielectric (quartz) tube embraced by the helicon antenna, which launches electromagnetic waves in the plasma. Electrons are heated through possibly collisional or Landau damping of the waves in the plasma. This process is not included self-consistently here; it is a subject of a separate study. In this model we assume that a certain power, W, is transmitted to the electrons. The electron temperature and density in the source are 6eV and 2x1012 cm-3, respectively, as measured in the ASPL experiments [5, 19].

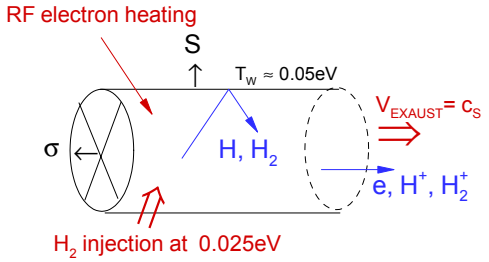

Let's accept the following physical model of a helicon plasma source, as shown in Fig.16. Next, we consider the ac esses taking

Fig.16. Helicon discharge model

Electron and ion transport. The electrons are magnetized by a relatively strong magnetic field of 0.1-0.6T. The electron gyroradius is about 10-2cm, ion gyroradius – 0.2cm, which is much smaller than 10cm-tube's diameter. The gyroradius becomes huge in the nozzle. Cross-field transport is weak because of the low plasma density. The plasma flux onto outer wall is negligible. Electrons strictly follow field lines, which are parallel to the cylinder axis. At one of the tube's ends there is a floating potential wall. The floating potential value for hydrogen (deuterium) plasma is 2.8(3) Te. Thus, the majority of the electrons are reflected back. There is a small residual particle/energy flux onto the end plate. We anticipate that the continuous puffing of H2 through the inlet will keep the plasma density low near the end plate. Therefore, we neglect the heat and mass flow onto the floating end plate. At the open end of the quartz tube the plasma is leaving the system at a fraction of sound speed.

Plasma exhaust velocity. The Debye length of the plasma in typical Helicon hydrogen discharge, λD, is on the order of 10-3 cm, while the tube dimension is on the order of 1m. Therefore, plasma in the volume is quasineutral and the plasma flow is ambipolar. We assume that the ion's exhaust velocity is sub-sonic with a fraction of the ion sound speed, CSi=(2Te/Mi)0.5. The electron density is equal to the combined density of all ion species (H+, H2+, H3+ here). The electron exhaust velocity is such to automatically maintain the ambipolarity of plasma Ve=(nH+CSH++nH2+CSH2++nH3+CSH3+)/ (nH++nH2++ nH3+). Neutral exhaust velocity is assumed to be sub-sonic as well with CSN≈0.03 (2TN/MN)0.5. Because the neutral temperature is significantly lower than the electron temperature, ions exhaust the helicon source at a much higher pace than the cold neutrals.

Energy exhaust and wall fluxes. Sonic neutral exhaust carries along energy flux:

$$Q^E = \sigma j^E (CkT + \frac{1}{2} M C_S^2) = \sigma (C+1) nkT \; V_T \qquad (10)$$

where σ is a quartz tube cross-section, VT is thermal velocity, C is specific heat. Wall neutral flux requires separate attention. We assume that gas (and plasma) has Maxwellian distribution:

$$f_M(n,T) = \frac{n}{(\pi^{1/2} V_T)^3} \cdot \exp\left\{-\frac{v^2}{V_T^2}\right\} \qquad (11)$$

and fills the tube homogeneously. We may easily find the kinetic energy and particle fluxes onto wall to be:

$$q^W(n,T) = \int_{-\infty}^{+\infty}\int_{-\infty}^{+\infty}\int_{0}^{+\infty} v_x \frac{Mv^2}{2} f_M dv_x dv_y dv_z =$$

$$\frac{nMV_T^3}{\pi^{3/2}} \int_0^{+\infty}\int_0^{+\infty} x \frac{x^2+p^2}{2} 2\pi p \cdot e^{-x^2-p^2} dx dp = \qquad (12)$$

$$\frac{nMV_T^3}{\pi^{1/2}} 2 \int_0^{+\infty}\int_0^{+\infty} \frac{1}{4} r e^{-r-s} dr ds = \frac{nkTV_T}{\pi^{1/2}}$$

and, respectively,

$$j^W(n,T) = \int_{-\infty}^{+\infty}\int_{-\infty}^{+\infty}\int_{0}^{+\infty} v_x f_M dv_x dv_y dv_z = \frac{1}{4} n V_T \qquad (13)$$

Note that this is just kinetic energy flux. Non-mono-atomic neutrals bringing also rotational energy to the wall. The expression for total energy deposited is

$$Q^W = (S+\sigma)(\alpha + \frac{C-1.5}{4}) \cdot nkTV_T \qquad (14)$$

where α=π-0.5. All particles that collide with wall are coming back with wall temperature TW≈500oC.

Temporal evolution of the density and temperature of the 6 plasma species: {*e*, H*2*, H, H+, H*2*+, H*3*+} is determined by cold gas puff rate, electron heating rate, energy exchange with wall, mass/energy exhaust and various inelastic collisional processes.

Inelastic collisions. We include the most important inelastic process caused by electron impact (electron mobility is highest). The energy structure of the hydrogen species as adopted to enforce conservation in present model is presented in Fig.17.

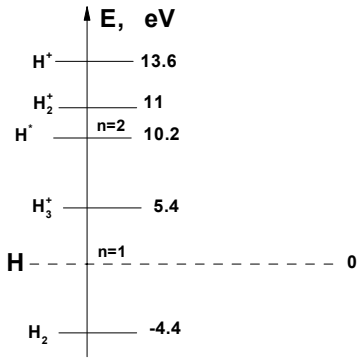

Hydrogen molecule dissociation (requires 4.4eV) by electron impact (rate DH2)

$$H2 + e \qquad H + H + e \qquad (15)$$

<IDH2> = <8.5,11.7,11.7 eV> ≈ 10eV. We assume the electron loses 10eV and each H atom carries away H2 /. Fig.17. Energy levels of hydrogenic species

Hydrogen molecule ionization by electron impact (rate IH2)

$$H2 + e \qquad e + H2+ + e \qquad (16)$$

*E*lectron loses I IH2= 15.4 eV, secondary electron is created with 0eV energy, H*2*+ carries away all H2 energy.

Molecular hydrogen ion dissociation (takes 2.6eV) by electron impact (rate DH2+)

$$H2+ + e \qquad e + H+ + H \qquad (17)$$

{From averaged vibrational states I=2.4 eV, atom and atomic ion carry away extra <E>=4.3eV each in theory}
We assume electron loses IDH2+=11.2eV, and that atom and ion carry away H2 /2 + 1/2EDH2+(=8.6eV) apiece.

Hydrogen atom ionization by electron impact (rate IH)

$$H + e \qquad e + H+ + e \qquad (18)$$

Electron loses IIH = 13.6eV, secondary electron at 0eV
H+ carries H energy.

Hydrogen atom excitation by electron impact (rate EH)

$$H + e \qquad e + H^*(n=2) \qquad e + H + \gamma \qquad (19)$$

Electron loses IEH = 10.2eV, energy ZEH (=10.2 eV) radiated as Lyman-α.

Heavy ion formation (only non-electron reaction) (rate FH3)

$$H2+ + H2 \qquad H3+ + H \qquad (20)$$

Exothermic reaction with EFH3 = 1.2eV, evenly divided between products.
We add the following comment on the included plasma processes. If plasma temperature is low at about 1eV then negative ions H- and vibrational-rotational levels dynamics of H*2*(v,j), H*2*+(v,j) may be important. Other excited levels of H (n=3,4,..) may be important if plasma density goes up. Among other elementary processes to be of importance: resonance charge-exchange H2-H2+ and H-H+, 3-body and photo recombination, Coulomb collisions, inter- and intra- elastic collisions between neutral particles and ions. Another interesting possibility is H3+ ion formation, but this is non-electron reaction. As plasma density is low ~1012 cm-3 and temperature is moderate Te~6eV, we think that 5 mentioned reactions will be dominating.

Set of balance equations

We are in position of deriving equations for plasma and gas density and temperature. Analysis shows that

instead of temperature it's better to introduce energy density q=CnT. In this case relative equations are simpler and explicitly express energy conservation (while density equation preserves mass). By looking on reaction rates [9-10] (Fig.18) and product energies, we can draw the following conclusions:

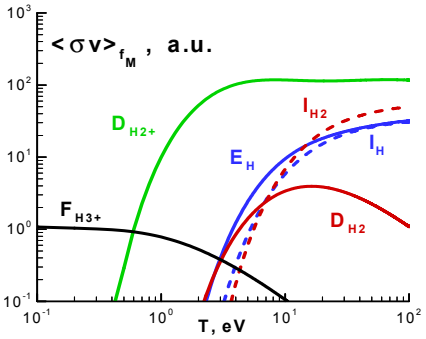

Fig.8. Reaction rates vs T

1) There will be a large population of Frank-Condon neutrals (via both dissociation reactions). These neutrals will be effectively transporting heat to the wall because they are not magnetized and because tube radius is much smaller than its length. Exhaust velocity of such hot neutrals will be significantly higher than that of the cold neutrals. We'd like to simulate hot component more accurately. Therefore, we split atomic neutrals into two populations – cold, Hc, with temperature T⁓1eV and hot, Hh, with T 1-3eV Figure 18 - H-species reaction rates

2) Hydrogen atom excitation is more probable than ionization. So, a significant fraction of energy can be radiated as Lyman-α. Plasma is optically thin, and all radiated power will be absorbed by internal elements (antenna, etc.). Molecular ionization has slightly higher cross-section and also energy threshold if compared to atomic hydrogen. This tells that there might be a significant fraction of H*2*+ ions (and possibly H*3*+) in the discharge, depending on the H/H*2* ratio.

The system of equations has to be normalized by choosing an appropriate set of dimensionless units (typical length is 1m and thermal velocity of 1eV atom). The following units are adopted: [n]=1013*cm*-3, [σk]=10-16cm2, [T]=[E]=1*eV*, [L]=1*m*, [m]=Mp (proton mass). We may find other units to be [V]=(2*eVk*/M)1/2, [t]=[L]/[V]≈0.7ms, [W]=[T]/[t], [R]=1/[n][t], etc.

Equation for cold molecule density includes gas puff, molecular dissociation and excitation, particle exhaust. Equation for energy density contains related energy sinks/sources and also energy conversion at the inner wall. We presented only expression for ionization rate. The rest are obtained in a similar way. We keep calculated rates in a tabulated form to eliminate need for their re-calculation during simulation. In these units the final form of the equations for H2c mass and energy density are:

$$\frac{dn_{H2c}}{dt} = \frac{\mu}{\sigma L} - D_{H2} n_e n_{H2c} - I_{H2} n_e n_{H2c} + F_{H3} n_{H2+} n_{H2c} - \gamma^A_{H2c} n_{H2c} V_T^{H2c}$$

$$\gamma^A_{H2c} = \frac{1}{L}$$

$$I_{H2}(T_e) = \frac{0.1}{n_e} \cdot \int_0^\infty 4\pi v^3 \sigma_{IH2} f_M^e(n_e, T_e) dv$$

$$\frac{dQ_{H2c}}{dt} = \frac{\mu}{\sigma L} Q_{H2} T^0_{H2} - (D_{H2} n_e + I_{H2} n_e + F_{H3} n_{H2+}) Q_{H2c} - \delta^A_{H2c} Q_{H2c} V_T^{H2c} + \delta^B_{H2c} T^W n_{H2h} V_T^{H2h} \quad (21)$$

$$\delta^A_{H2c} = \frac{(S+\sigma)}{\sigma L} \cdot (\alpha + \frac{C_{H2h} - 1.5}{4}) + \frac{1}{L} \cdot (C_{H2h} + 1)$$

$$\delta^B_{H2c} = \frac{C_{H2c}(S+\sigma)}{4\sigma L}, \quad C_{H2c} = \frac{5}{2}$$

$$T_{H2c} = Q_{H2c} / C_{H2c} n_{H2c}$$

$$V_T^{H2c} = \sqrt{T_{H2c}/2}$$

The equations for the rest 6 plasma components can be easily obtained using similar approach. In the final dimensionless form they read are as follows. For molecular ions:

$$\frac{dn_{H2+}}{dt} = I_{H2} n_e n_{H2c} - D_{H2+} n_{H2+} n_e$$
$$- F_{H3} n_{H2+} n_{H2} - \gamma_{H2+} n_{H2+} C_S^{H2+}$$
$$\gamma_{H2+} = \frac{1}{L}$$
$$\frac{dQ_{H2+}}{dt} = I_{H2} n_e Q_{H2c} \qquad (22)$$
$$- (D_{H2+} n_e + F_{H3} n_{H2}) Q_{H2+}$$
$$- \delta^A_{H2+} n_{H2+} T_{H2+} C_S^{H2+} - \delta^B_{H2+} n_{H2+} T_e C_S^{H2+}$$
$$\delta^A_{H2+} = \frac{C_{H2+}}{L} \quad , \quad \delta^B_{H2+} = \frac{1}{L}$$
$$T_{H2+} = Q_{H2+} / C_{H2+} n_{H2+}, \quad C_{H2+} = \frac{5}{2}$$
$$V_T^{H2+} = \sqrt{T_{H2+}/2}, \quad C_S^{H2+} = \sqrt{T_e/2}$$

Equations for cold neutrals has extra particle source at the wall due to hot neutrals interacting with the wall:

$$\frac{dn_{Hc}}{dt} = -I_H n_e n_{Hc} + \gamma^A_{Hc} n_{Hh} V_T^{Hh} - \gamma^B_{Hc} n_{Hc} V_T^{Hc}$$
$$\gamma^A_{Hc} = \frac{\sigma + S}{4L\sigma}; \quad \gamma^B_{Hc} = \frac{1}{L}$$
$$\frac{dQ_{Hc}}{dt} = -I_H n_e Q_{Hc} - \delta^A_{Hc} n_{Hc} T_{Hc} V_T^{Hc}$$
$$+ \delta^B_{Hc} n_{Hh} T^W V_T^{Hh} \qquad (23)$$
$$\delta^{\mathrm{A}}_{Hc} = \frac{(S+\sigma)}{\sigma L} \cdot (\alpha + \frac{C_{Hc} - 1.5}{4}) + \frac{1}{L} \cdot (C_{Hc} + 1)$$
$$\delta^B_{Hc} = \frac{C_{Hc}(S+\sigma)}{4\sigma L}$$
$$V_T^{Hc} = \sqrt{T_{Hc}}$$
$$T_{Hc} = Q_{Hc} / C_{Hc} n_{Hc}, \qquad C_{Hc} = \frac{3}{2}$$

Equations for hot neutral account for doubled rate of hot neutrals production during molecule dissociation and their conversion to cold neutrals at the wall.

$$\frac{dn_{Hh}}{dt} = -I_H n_e n_{Hh} + 2D_{H2} n_e n_{H2c} + F_{H3} n_{H2} n_{H2+}$$
$$+ D_{H2+} n_e n_{H2+} - \gamma_{Hh} n_{Hh} V_T^{Hh}$$
$$\gamma_{Hh} = \frac{S + 5\sigma}{4\sigma L} \qquad (24)$$
$$\frac{dQ_{Hh}}{dt} = -I_H n_e Q_{Hh} + D_{H2} n_e (Q_{H2c} + n_{H2c} E_{DH2})$$
$$+ 0.5 D_{H2+} n_e (Q_{H2+} + n_{H2+} E_{DH2+})$$
$$+ 0.5 F_{H3} (n_{H2} Q_{H2+} + n_{H2+} Q_{H2+} + n_{H2+} n_{H2} E_{FH3})$$
$$- \delta_{Hh} Q_{Hh} V_{Hh}^T$$
$$\delta_{Hh} = \frac{(S+\sigma)}{\sigma L} \cdot (\alpha + \frac{C_{Hh} - 1.5}{4}) + \frac{1}{L} \cdot (C_{Hh} + 1)$$
$$V_T^{Hh} = \sqrt{T_{Hh}}$$
$$T_{Hh} = Q_{Hh} / C_{Hh} n_{Hh}, \qquad C_{Hh} = \frac{3}{2}$$

Atomic ion equations account for ionization of hot and cold atomic hydrogen, dissociation of molecular ions and ion loss through the nozzle:

$$\frac{dn_{H+}}{dt} = I_H n_e (n_{Hh} + n_{Hc}) + D_{H2+} n_e n_{H2+}$$
$$- \gamma_{H+} n_{H+} C_S^{H+}; \qquad \gamma_{H+} = \frac{1}{L}$$
$$\frac{dQ_{H+}}{dt} = I_H n_e (Q_{Hh} + Q_{Hc}) +$$
$$0.5 D_{H2+} n_e (Q_{H2+} + n_{H2+} E_{DH2+}) \qquad (25)$$
$$- \delta^A_{H+} n_{H+} T_{H+} C_S^{H+} - \delta^B_{H+} n_{H+} T_e C_S^{H+}$$
$$\delta^{\mathrm{A}}_{H+} = \frac{1}{L} \cdot C_{H+}, \quad \delta^B_{H+} = \frac{1}{L}$$
$$V_T^{H+} = \sqrt{T_{H+}}, \quad C_S^{H+} = \sqrt{T_e}$$
$$T_{H+} = Q_{H+} / C_{H+} n_{H+}, \quad C_{H+} = \frac{3}{2}$$

Heavy ion equations balance H3+ ion production and their exhaust into the nozzle:

$$\frac{dn_{H3}}{dt} = F_{H3} n_{H2} n_{H2+} - \gamma_{H3} n_{H3} C_S^{H3}$$

$$\gamma_{H3} = \frac{1}{L}$$

$$\frac{dQ_{H3}}{dt} = 0.5 F_{H3} (n_{H2} Q_{H2+} + \quad (26)$$

$$n_{H2+} Q_{H2} + n_{H2+} n_{H2} E_{F3})$$

$$- \delta_{H3}^{A} n_{H3} T_{H3} C_S^{H3} - \delta_{H3}^{B} n_{H3} T_e C_S^{H3}$$

$$\delta_{H3}^{A} = \frac{1}{L} \cdot C_{H3}, \quad \delta_{H3}^{B} = \frac{1}{L}$$

$$V_T^{H3} = \sqrt{T_{H3}/3}, \qquad C_S^{H3} = \sqrt{T_e/3}$$

$$T_{H3} = Q_{H3} / C_{H3} n_{H3}, \quad C_{H3} = 2$$

Finally, density equation for electron because of the quasineutrality constraint reduces to a simple form. At the same moment energy density equation is the most elaborate. It accounts for all inelastic processes included into plasma chemistry kinetic, electron heating and electron energy carried by ion sub-sonic flow.

$$n_e = n_{H+} + n_{H2+} + n_{H3+}$$

$$\frac{dQ_e}{dt} = \frac{W}{\sigma L} - n_e I_{DH2} D_{H2c} n_{H2c}$$

$$- n_e I_{IH2} I_{H2c} n_{H2c} \quad (27)$$

$$- n_e I_{DH2+} D_{H2+} n_{H2+}$$

$$- n_e I_{IH} (I_{Hh} n_{Hh} + I_{Hc} n_{Hc})$$

$$- n_e I_{EH} (E_{Hh} n_{Hh} + E_{Hc} n_{Hc})$$

$$- \delta_e T_e (n_{H+} C_S^{H+} + n_{H2+} C_S^{H2+} + n_{H3} C_S^{H3})$$

$$\delta_e = \frac{1}{L} \cdot C_e, \quad C_e = \frac{3}{2}$$

$$T_e = Q_e / C_e n_e$$

For monatomic particles we used following values of specific heat coefficients: C=1.5, for diatomic species C=2.5, and for heavy ions C=3.

Benchmarking against analytical results. For relaxation oscillations see ref. [20].

Benchmarking against VX-3 experimental data.

We performed runs for the following fixed parameters of the helicon deuterium discharge: R=5cm, L=70cm, TW=0.05eV, T0=0.03eV. We have varied input power about W=1-2.5kW and mass of puffed gas, μ=50-130sccm. We tried to be close to experimental data: Te=5-7eV, n=1-2x1012cm-3. Best agreement was achieved under the following assumptions [16]:
(a) mean gas flow in the source is sub-sonic at M=0.03;
(b) plasma ‘’parallel’’ flow velocity VZ=0.3Cs;
(c) electrons absorb 40% of input power.

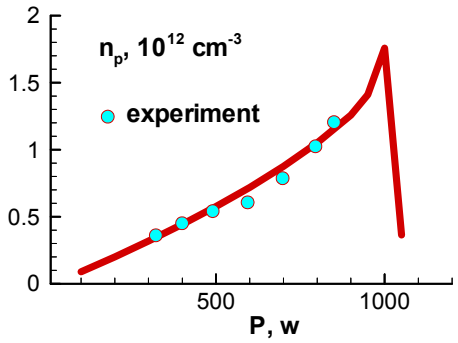

Figure 19 - np vs P

In the Fig. 20 plasma density scan versus gas flow rate at fixed input power is presented. Numerical model

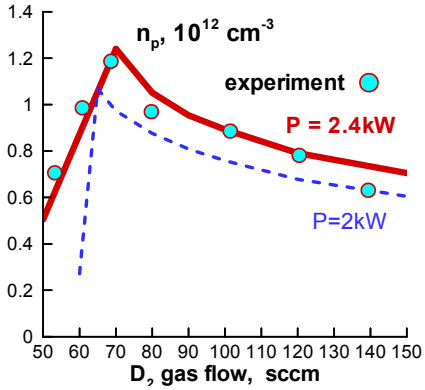

Figure 20 - np vs μ

Figure 19 illustrates dependence of the plasma density versus absorbed RF-power. Agreement between simulation (solid curve) and experiment is better than 10%. Numerical model explains why plasma density goes up faster than the input power. It turns out that

electron temperature goes up, making the fraction of the energy that goes into gas ionization higher with respect to radiation (Ly-α) loses.
As one can see, the 0-D mass-power balance model reproduces VX-3 experimental data quite well. The only difference is observed beyond certain input power per unit mass throughput. In the simulation we see that discharge either decays or oscillates. However, in the lab experiment this phenomenon was never observed.

Effect of a residual gas pressure in the vacuum tank.

We suspected that the finite gas density was responsible to the phenomenon just described. To prove it we have performed two runs with the same input power, but different conditions. In the first run no neutrals were coming into discharge from the vacuum tank, while in the second it was a background gas pressure at 1mtor. This pressure is measured in the experiment, at room temperature it corresponds to the N≈1013cm-3gas density.

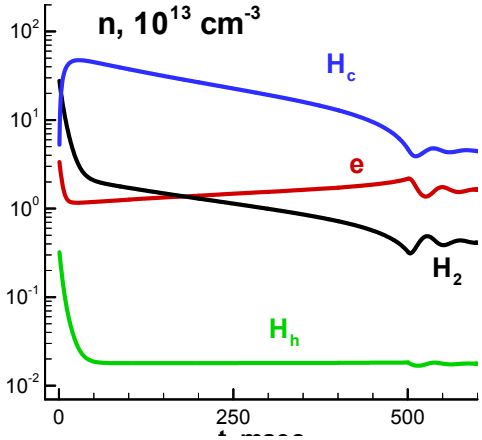

Figure 21 – in space

From the Fig.21 one can see that discharge in the vacuum (in the space) is unstable, while background pressure stabilizes it (Fig.22). This effect can be critical for the VASIMR thruster design and operation in the orbit.

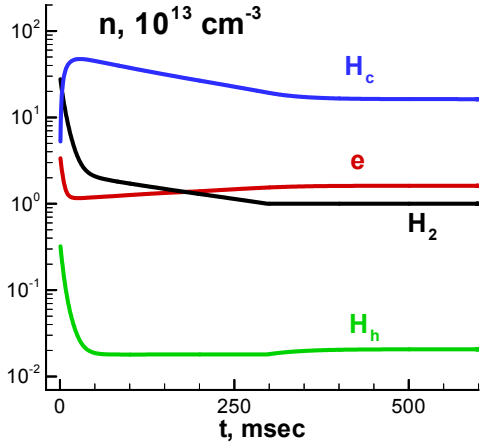

Figure 22 - in the lab

Study of the operation of the VF-10 plasma source.

VF-10 has larger and more powerful plasma source.
We in position to apply our 1-D and 0-D models to the hydrogen discharge with the VF-10 parameters:
d=10cm, L=100cm, μ=1mg/sec(≈670sccm), P=10kW.
The prediction from the hybrid gas flow model reads as follows [20]:
a) required pressure drop inlet-vacuum chamber is ~430 mtorr, ΔP~25 mtorr in the tube along;
b) sizable ΔP~2 mtorr pressure loss in the magnet bore.
c) mean Mach number of the flow <M>~0.07 (was 0.03 for VX-1kW).
Key plasma conditions for the VF-10 configuration will be discussed in the connection with proposed baffles later in this paper**.**

Effect of the propellant preheating.

To gain efficiency it was proposed to use gas preheating for the helicon source. We used VF-10 parameters to perform analysis of hydrogen pre-heating. Temperature of the gas in the inlet was varied in the 20-1000oC range, while al the rest parameters were kept the same. Input profiles of gas temperature distribution and the resulting profiles of gas density are shown in Fig. 23. Dependencies of the averaged gas density, N, required pressure in the inlet, PI, to drive the gas, and mean velocity of gas flow in the quartz tube are presented in Fig.24. One can see, that has preheating gives rise to gas exhaust, which ultimately decreases fuel utilization efficiency. It also

reduces gas density in the source, which in turn leads to the drop in plasma density.

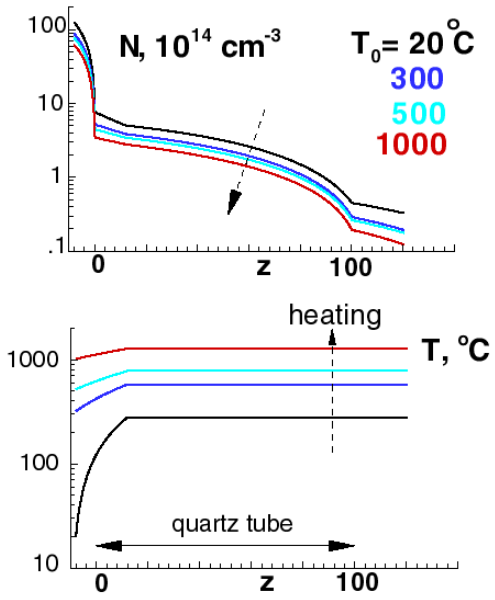

Figure 23 – Evolution of T and N profiles

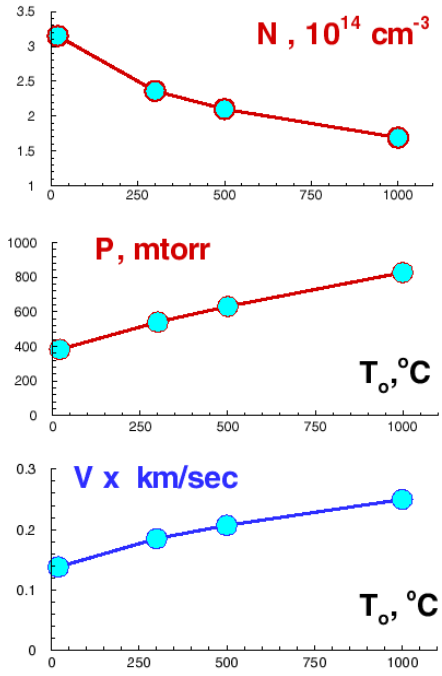

Figure 24 – Gas flow parameters vs To

Explanation of the effect of pressure jump in the inlet. The jump was observed in the experiment as RF-power was switched on in the VX-1 experiment. Relative increase in pressure for the hydrogen is about 30-40%. We find that at least 20% can be easily explained due to gas heating during discharge. As gas temperature goes up, gas viscosity increases. As a result larger pressure drop is required to drive the same constant amount of gas through the system. In Fig.25 we present results for hydrogen flow at μ= 60 and 80 sccm. As one can see for the measured quartz tube temperature jump (ΔTQT≈260oC), corresponding relative pressure jump in the inlet ΔP/P≈20%. This estimate does not take into account energetic Frank-Condon neutrals, which may add another 10-15% to the pressure jump. Note that actual gas temperature may differ from quartz tube T.

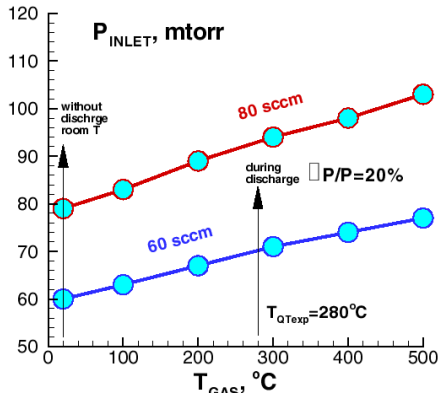

Figure 25 – ΔP vs To

Internal baffles (along with magnetic field choke) have been proposed to retain propellant in the plasma source. The quantitative effect of baffles can be easily included into the system of equation (21-27) by reducing by a certain factor coefficients γ and δ in the equation for neutral species.

In Fig. 26 a), b), and c) we present results for the VF-10 configuration with no baffle, medium 1:3.5 and large 1:7 ratio. As one can see for the same lower input (absorbed ~1-2kW) RF-power plasma density is lower for the cases with baffles. Energy efficiency also drops with baffles. The reason is the following. Electron temperature drops with baffles. As a result ratio of radiated power to the useful (gas dissociation and ionization) goes up. The only benefit of the baffles introduction is the possibility to sustain stable discharge at higher input RF-power.

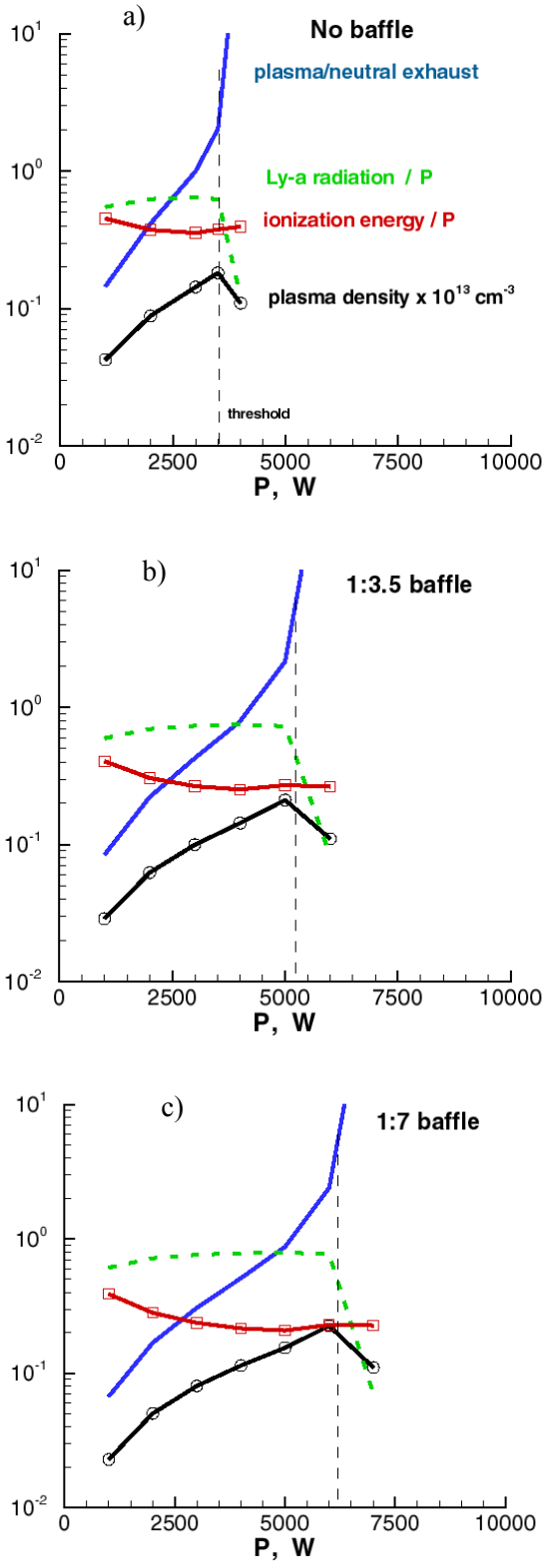

Figure 26 – Key discharge parameters vs input RF power, P, for 3 cases: a) – no baffle, b) – 1:3.5, and c) - 1:7 gas baffle

From the helic

utilization efficiency exceeds 50%. However, this regime is close to the discharge stability limit and requires fine-tuning. Such regime (Fig.26a) may also yield ~30% efficiency of the applied power utilization.

Catalytic break of H2 gives another possibility to alter helicon source performance.

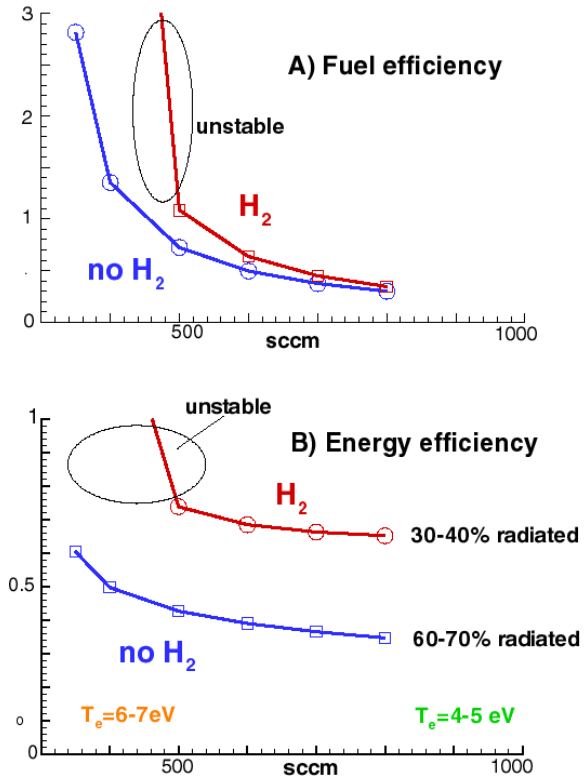

Figure 27 – Mass scans of "fuel" (A) and energy (B) efficiencies for with (no H2) and without (H2) catalytic brake of molecules

Direct comparison of discharges with and without catalytic pre-dissociation of the hydrogen molecules (Fig.27A and B) indicates that without molecules discharge loses almost 50% of its efficiency. The physical explanation is in the fact that radiation is the major energy loss. Because the electron temperature is about 6-7eV, rate of direct ionization of the hydrogen molecule can exceed rate of the molecule dissociation. As the result atomic hydrogen fraction reduces, causing reduction of the plasma radiation.

Effect of radiation reduction and re-capture.

To study these new effects the energy balance equations (21-27) were modified in the following

ways: a) the effective cross-section of a hydrogen atom excitation by electron impact was gradually reduced, and b) the cross-section stayed, but fraction of the radiation was re-captured through the ionization channel.

The discharge parameters scan versus radiation fraction is presented in the Fig. 28 for the reduction model.

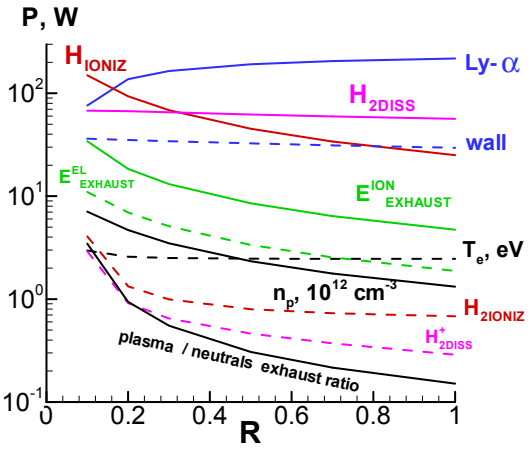

Figure 28 – Helicon hydrogen discharge parameters vs fraction, R, lost due to Ly-α radiation (electron impact excitation).

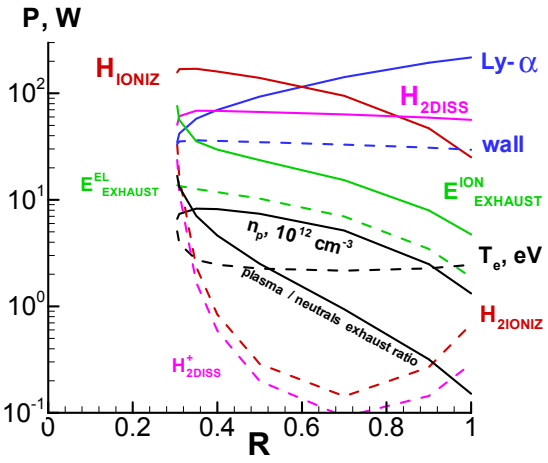

Figure 29 – Helicon hydrogen discharge parameters vs fraction, R, lost due to Ly-α radiation. 1-R part is re-captured by plasma

Similar curves for the recapture model are shown in the Fig.29. As one can see, some 80% radiation reduction or just 40% radiation recapture allows to achieve more than 50% energy efficiency, while gas utilization efficiency can easily jump up to 60-70%.

Fully kinetic model of the VASIMR thruster

Much more elaborate 1D2V Fokker-Planck model for VASIMR thruster plasmas was discussed in the previous works [12, 16, 27]. Presently we are trying to extend it to more dimensions, by adding cross-field terms into the corresponding kinetic equation, and coupling plasma equations with the kinetic equation for neutral gas.

Meanwhile, we are in position to compare 1D2V kinetic results for ion distribution function [16] to the recent RPA data [21].

Kinetic simulation for two-component plasma shows that the electron distribution function [16] is close to Maxwellian (has to be also compared to the gas result in Fig.15). However, the ion distribution (IDF, shown in Fig.30) is very non-equilibrated. This happens due to many factors, including magnetic field trapping effect, acceleration in the anomalous axial ambipolar potential, and collisions.

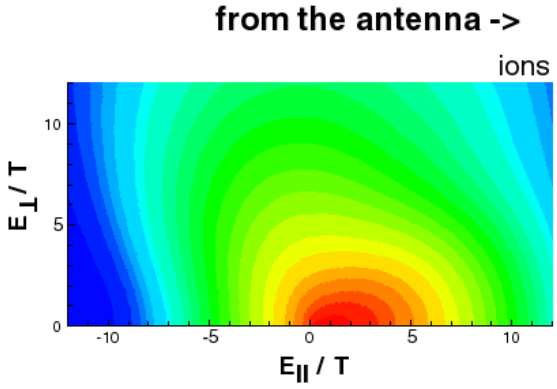

Figure 30 – IDF as calculated by the fully kinetic model

Simul on with ely high specific impulse of about 6-8Ksec for quite moderate input powers ~4kW.

Resent experimental data from the VX-10 RPA show that specific impulse of about 4Ksec for the 3kW input power. Interestingly enough, the kinetic model results are close to that obtained recently is the ASPL (Advanced Space Propulsion Laboratory, Houston) experiment [21] (see the measured ion distribution function in Fig.31).

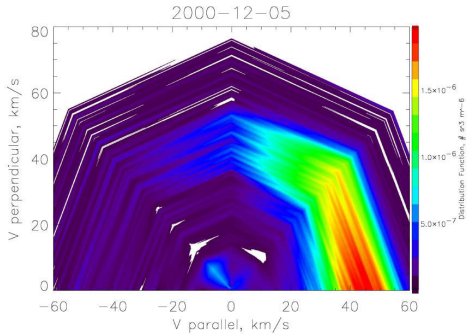

Figure 31 – IDF as measured by RPAs in the VX-10 VASIMR configuration

Conclusions

Several models to study propellant flow and plasma conditions in the helicon source of VASIMR thrusters have been developed. The models have been benchmarked against experimental data of the VX-10 experimental setup. Numerical results demonstrate good agreement with the lab data. The models are used to study numerous effects in the VASIMR thrusters: radiation reduction and recapture, role of baffles and vacuum tank effect, gas pre-heating and catalytic dissociation, etc. We propose modification of source by using conical-shaped quartz tubes.
Results from the kinetic modeling are in agreement with simple semi-analytical models. Kinetic simulations indicate that gas distribution function can differ from the Maxwellian. Ion distribution function strongly deviates from the equilibrium, and is in agreement with resent RPA data from the VX-10 experiment. Latest result suggest that the VASIMR helicon plasma source can yield specific impulse on the order of 4-8Ksec, and therefore may serve as an effective electrical propulsion system along.

Acknowledgements

This work is supported by NASA Houston L. Johnson Space Center.

References

[1] Chang Díaz F.R., "Research Status of The Variable Specific Impulse Magnetoplasma Rocket", *Proc. 39th Annual Meeting of the Division of Plasma Physics* (Pittsburgh, PA, 1997), *Bulletin of APS*, **42,** 2057, 1997.

[2] Chang Díaz, F. R., Squire, J. P., Carter, M., et al., ''Recent Progress on the VASIMR'', *Proc. 41th Annual Meeting of the Division of Plasma Physics* (Seattle, WA, 1999), *Bulletin of APS*, **44**, 99, 1999.

[3] Chang Díaz, F. R., Squire, J. P., Ilin, A. V., et al. "The Development of the VASIMR Engine", *Proceedings of International Conference on Electromagnetics in Advanced Applications (ICEAA99), Sept. 13-17, 1999*, Torino, Italy, 99-102, 1999.

[4] F.R.Chang Diaz et al., "An Overview of Current Research on the VASIMR Engine", DPP-2000, Bull. APS, vol.45 (7) 129, 2000.

[5] J.P.Squire, "Recent Experimental Results in the VX-10 Device", DPP-2000, Bull. APS, vol.45 (7) 130, 2000.

[6] Braginskii, S.I., ''Transport Processes in Plasmas'' in *Reviews Plasma Phys*., vol.1, Consultants Bureau, NY, 205, 1965.

[7] A.V.Nedospasov and M.Z.Tokar, "Wall Plasma in Tokamaks", in Reviews of Plasma Physics, Ed. Acad. B.B.Kadomtsev, Consultants Bureau, N.Y. v.18, p.77, 1993.

[8] Chen, F.F., "Plasma Ionization by Helicon Waves", *Plasma Physics and Control Fusion*, **33**, 339-364, 1991.

[9] Janev, R.K., Langer, W.D., Evans, K., Post, D.E "Elementary Processes in Hydrogen-Helium Plasmas", *Springer-Verlag*, Berlin, 1987.

[10] "Atomic and Molecular Processes in Fusion Edge Plasmas", ed. R.K.Janev, Plenum Press, N.Y. , 1995.

[11] Batishchev O., Shoucri M., Batishcheva A., Shkarofsky I., ''Fully Kinetic Simulation of Coupled Plasma and Neutral Particles in Scrape-Off Layer Plasmas of Fusion Devices'', J. Plasma Phys. **61**, 347-364, 1999.

[12] Batishchev, O ''Kinetic Model for the Variable Isp Thruster'', *Proc. 41th Annual Meeting of the*

Division of Plasma Physics (Seattle, WA, 1999), *Bulletin of APS*, **44** , 99, 1999.

[13] L.B.Loeb, "The kinetic theory of gases", Dover Publications Inc., N.Y. , 1961.

[14] Schlichting H., "Boundary-Layer Theory", 7th Edition, McGraw-Hill, Inc., 1987.

[15] S.Chapman and T.G.Cowling, "The mathematical theory of non-uniform gases", Univ. Printing House, Cambridge, 1970.

[16] O.Batishchev and K.Molvig, "Kinetic Simulation of the high Isp Plasma Thruster", JPC-36, AIAA-3754 technical paper, -11p. , 2000.

[17] O.Batishchev and K.Molvig, "Study of the Operational Regimes of the VASIMR Helicon Plasma Source", DPP-2000, Quebec City, Canada, Bull. APS, 45 (7) 130, 2000

[18] O.Batishchev and K.Molvig, "Study of Mixed Collisionality Gas Flow in the VASIMR Thruster", DFD-2000, DC, USA, Bull. APS, 45 (9) 169, 2000.

[19] J.P.Squire, Private Communication, 2001, and 4th VASIMR Workshop, Houston, March, 2001.

[20] O.Batishchev and K.Molvig, "Kinetic Model of helicon plasma source for VASIMR", ACME-39, Reno, AIAA-2001-0963 technical paper, -12p., 2001.

[21] E.Bering, Private Communication, 2001, also at ACME-39, Reno, January, 2001.

[22] O.Batishchev et al, "Kinetic Effects in Tokamak Scrape-off Layer Plasmas" *Physics of Plasmas* **4** (5), 1672, May 1997

[23] O.V.Batishchev, A.A.Batishcheva, A.S. Kholodov "Unstructured adaptive grid and grid-free methods for magnetized plasma fluid simulations", *J. Plasma Phys.* **61**, part 5, 701, 1999.

[24] O.Batishchev and Kim.Molvig, "Kinetic model for a mixed collisional rarified gas flow", In. Proc. 1St MIT Conf on CFD, Cambridge, MA, USA, June 12-15, 2001.

[25] O.Batishchev and Kim.Molvig, "Modeling of a helicon plasma source" , Proc. PPPS-2001 Conf., p.157, Las Vegas, NV, USA, June 17-21, 2001.

[26] O.Batishchev and Kim.Molvig, "Numerical study of a helicon gas discharge" , Annual Meeting APS DcomP, D2.006., Cambridge, June 25-28, 2001.

[27] O.Batishchev and Kim.Molvig, "Kinetic Study of the VASIMR thruster operational regimes", AIAA technical paper AIAA-20001-3501, -14p, 2001.

[28] B.F.Armaly, F.Durst, J.C.F.Pereira, B.Schonung "Experimental and theoretical investigations of backward-facing step flow", J. Fluid Mech., **127**, 473-496, 1983.